Informing Deep Argo Array Design Using Argo and Full-Depth Hydrographic Section Data*

GREGORY C. JOHNSON

NOAA/Pacific Marine Environmental Laboratory, Seattle, Washington

JOHN M. LYMAN

NOAA/Pacific Marine Environmental Laboratory, Seattle, Washington, and Joint Institute for Marine and Atmospheric Research, University of Hawai'i at Mānoa, Honolulu, Hawaii

SARAH G. PURKEY

Lamont-Doherty Earth Observatory, Columbia University, Palisades, New York

(Manuscript received 7 July 2015, in final form 19 August 2015)

ABSTRACT

Data from full-depth closely sampled hydrographic sections and Argo floats are analyzed to inform the design of a future Deep Argo array. Here standard errors of local decadal temperature trends and global decadal trends of ocean heat content and thermosteric sea level anomalies integrated from 2000 to 6000 dbar are estimated for a hypothetical 5° latitude × 5° longitude × 15-day cycle Deep Argo array. These estimates are made using temperature variances from closely spaced full-depth CTD profiles taken during hydrographic sections. The temperature data along each section are high passed laterally at a 500-km scale, and the resulting variances are averaged in 5° × 5° bins to assess temperature noise levels as a function of pressure and geographic location. A mean global decorrelation time scale of 62 days is estimated using temperature time series at 1800 dbar from Argo floats. The hypothetical Deep Argo array would be capable of resolving, at one standard error, local trends from <1 m °C decade^{-1} in the quiescent abyssal North Pacific to about 26 m °C decade^{-1} below 2000 dbar along 50°S in the energetic Southern Ocean. Larger decadal temperature trends have been reported previously in these regions using repeat hydrographic section data, but those very sparse data required substantial spatial averaging to obtain statistically significant results. Furthermore, the array would provide decadal global ocean heat content trend estimates from 2000 to 6000 dbar with a standard error of ±3 TW, compared to a trend standard error of ±17 TW from a previous analysis of repeat hydrographic data.

1. Introduction

The international Argo program (Roemmich et al. 2009) reports over 100 000 upper-ocean profiles of temperature and salinity per year. The Argo array first achieved its target of 3000 freely drifting autonomous CTD-equipped floats in November 2007. Argo floats drift with the currents at a nominal pressure of 1000 dbar, leaving that isobar nominally every 10 days to profile between a target pressure of 2000 dbar and the surface, sampling as they ascend. The floats are nominally spaced at 3° × 3° intervals, and the array provides seasonally unbiased sampling around the globe for the upper half of the ocean volume, except in shallow (generally <1000–2000 dbar) or ice-covered waters. Argo is gradually expanding into seasonally ice-covered regions (Klatt et al. 2007), and ice-tethered profilers (Toole et al. 2011) have sampled regions of the Arctic between about 750 and 10 dbar since 2004.

However, the deeper half of the ocean volume below the 2000-dbar sampling limit of conventional Argo floats

* Pacific Marine Environmental Laboratory Contribution Number 4351 and Joint Institute for Marine and Atmospheric Research Contribution Number 15-391.

Corresponding author address: Gregory C. Johnson, NOAA/Pacific Marine Environmental Laboratory, 7600 Sand Point Way NE, Bldg. 3, Seattle, WA 98115.
E-mail: gregory.c.johnson@noaa.gov

DOI: 10.1175/JTECH-D-15-0139.1

is currently much more sparsely sampled. As of 7 July 2015, the World Ocean Database (http://www.nodc.noaa.gov/OC5/SELECT/dbsearch/dbsearch.html) contained 39 352 high-resolution CTD profiles with data extending to at least 3000 m for all time. For the year 2008 there were only 515 high-resolution CTD profiles with data extending to at least 3000 m in the database, mostly concentrated along a few densely sampled quasi-synoptic hydrographic sections, compared with 113 512 spatially and temporally well-distributed CTD profiles of the upper ocean from floats.

Regardless of data limitations, the abyssal ocean (here >4000-m depth) exhibited a detectible, albeit with large uncertainty, warming trend from 1992 to 2005 of about 5 m °C decade^{-1} in the global mean with deep (>2000 m) trends closer to 30 m °C decade^{-1} in the Southern Ocean (Purkey and Johnson 2010). The largest deep long-term warming trends we have found published are 130 m °C decade^{-1} from 1980 to 2010 estimated from repeated measurements in the deep Greenland Sea (Somavilla et al. 2013). This latter trend is similar in magnitude to the global average trend in sea surface temperature warming from 1970 to 2014 (~115 m °C decade^{-1}) using the NOAA ERSST analysis (Smith et al. 2008). Deep variability in temperature and salinity can reflect variations in deep convection that connect the substantial heat capacity of the deep ocean directly to the ocean surface and also reflect changes in circulation. For instance, the deep Greenland Sea warming is a direct result of the cessation of deep wintertime convection in that region, with a resultant reversal in deep flow between the Greenland Sea and the Arctic Ocean (Somavilla et al. 2013). Variations in deep convection in locations such as the Labrador Sea (Yashayaev 2007) are likely to at least contribute in part to deep North Atlantic heat content variations (Mauritzen et al. 2012). The waters of southern origin that fill the majority of the deep and abyssal ocean (Johnson 2008) mostly cascade down in dense plumes from the Antarctic continental shelf (Orsi et al. 1999). However, open ocean convection in features such as the Weddell Polynya of the mid-1970s has also played a role (Gordon 1982) in ventilating the abyss in the Southern Ocean. The resulting Antarctic Bottom Waters (Orsi et al. 1999) spread north (Lumpkin and Speer 2007) and, as noted above, have been warming in recent decades (Purkey and Johnson 2010).

Ocean heat content increases account for over 90% of the warming in the earth's climate from 1971 to 2010 (Rhein et al. 2013). Globally, ocean heat content from 2000 to 6000 m has been estimated to increase during 1992–2005 from an analysis of repeat hydrographic data by the equivalent of 0.07 ± 0.03 W m^{-2} (uncertainty recalculated as one standard error of the mean) applied over the surface area of the earth (Purkey and Johnson 2010), similar to the rate of heat gain (equivalent to 0.06 ± 0.006 W m^{-2}) estimated deeper than 3000 m from 1985 to 2006 using data assimilation output (Kouketsu et al. 2011). The rate of observed ocean heat gain from 0 to 2000 m during 2006–13, when Argo sampling of the ice-free ocean is near global, is estimated at 0.5 ± 0.1 W m^{-2} (Roemmich et al. 2015). Deep ocean warming, at least for 1992–2005, amounts to about 14% of that value. Because the global ocean is only sparsely sampled at decadal intervals by repeat hydrographic sections (Talley et al. 2015), presently direct estimates of deep ocean heat content can only be made retrospectively over decadal time scales.

Attempts to estimate deep ocean temperature changes as a residual (sea level changes from satellite data minus ocean mass changes from satellite data minus the steric expansion from 0 to 2000 m from Argo data) are stymied by large uncertainties and can result in an inferred small and statistically insignificant residual cooling from 2005 to 2013 (Llovel et al. 2014) or residual warming over a similar period (Dieng et al. 2015) that the authors note could also be arising from changes in marginal and shallow seas undersampled by Argo. The variation in sign results mostly from differences in bias corrections for glacial isostatic adjustment and from the more general difficulty of inferring a relatively small value from the difference of larger ones. Thus, it is desirable to measure changes of deep ocean temperature (hence, heat content and steric expansion) directly, the better to close global heat budgets and local sea level budgets.

Changes in temperature are also related to changes in circulation. In a simple budgetary calculation, the warming of abyssal waters of potential temperature <0°C originating around Antarctica implies a reduction in the volume of these waters at a rate of around 8 Sv (1 Sv $\equiv 10^6$ m^3 s^{-1}) from 1992 to 2005 (Purkey and Johnson 2012), with an apparent slowdown of the northward flow of these waters across 35°S in the Pacific and western Atlantic at a rate of around 1 Sv decade^{-1} in each of those basins from 1968 to 2006 (Kouketsu et al. 2011). The Atlantic meridional overturning circulation also varies on a variety of time scales, with southward flow of lower North Atlantic Deep Water across 26°N slowing by 7% yr^{-1} from April 2004 to October 2012 (Smeed et al. 2014). These changes have obvious ramifications for the storage and cycling of heat, carbon, and other climate-relevant parameters, as well as sea surface temperatures (Cunningham et al. 2013) and even decadal climate prediction (Msadek et al. 2011; Yeager et al. 2012; Robson et al. 2012).

The renewed recognition of these dynamic, climate-relevant deep variations in temperature, salinity, and circulation below 2000 m has led to a call for a "Deep

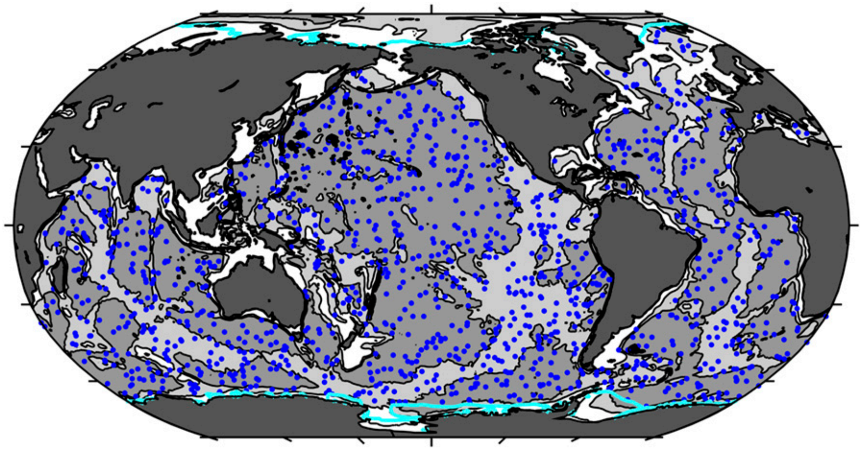

FIG. 1. Straw-plan of a nominally 5° × 5° distribution of 1228 Deep Argo floats (blue dots) randomly populating the global ocean excluding areas shallower than 2000 m (white areas), and areas with mean 1981–2010 ice concentrations >75% (poleward of thick cyan contours). Lightest gray areas indicate bottom depths between 2000 and 4000 m, darker gray areas indicate bottom depths exceeding 4000 m, and darkest gray areas indicate land.

Argo'' array (Johnson and Lyman 2014), to measure continuously the bottom half of the global ocean volume below 2000 m, currently sampled only sparsely at decadal intervals by repeat hydrography (Talley et al. 2015). Deep Argo floats require improvements in float and sensor technology. While 2000-dbar floats use aluminum cylinders for pressure cases, the 6000-dbar-capable Deep Argo floats use glass spheres because they better withstand high pressures and more closely match the compressibility of seawater, increasing energy efficiency. To detect the smaller signals in the deep ocean, CTDs used for Deep Argo will also require more accurate pressure (±3 dbar), temperature (±0.001°C), and salinity [±0.002; practical salinity scale 1978 (PSS-78)] measurements with 6000-dbar-capable sensors. In addition to these hardware improvements, to design an effective Deep Argo array, it is important to assess anticipated signals, noise levels, and scales of variability.

Here we use data mostly from a 1990s global survey of closely spaced hydrographic sections (WOCE) and repeats of a key subset of those sections during the 2000s (CLIVAR) and 2010s [Global Ocean Ship-Based Hydrographic Investigations Program (GO-SHIP)] along with data from Argo floats to inform the design of a future Deep Argo array. We estimate temperature variance in the deep (>2000 m) and abyssal (>4000 m) ocean using the hydrographic section data. We estimate decorrelation time scales (following von Storch and Zwiers 1999) from quasi-Lagrangian Argo float temperature time series at 1800 m. A global mean deep horizontal decorrelation length scale of 160 km has already been estimated in a similar manner using temperature data from 28 repeated hydrographic sections, each spanning at least 2000 km (Purkey and Johnson 2010). Hence, as long as Deep Argo floats are separated by more than 160 km, each can be assumed to provide spatially independent information. In section 2 we detail the data used and their processing. In section 3 we detail the analyses performed, including assessments of decorrelation time scales, the detection limits for global decadal trends, and the estimated uncertainties of global integrals of annual ocean heat content anomalies for a relatively sparse (5° × 5° × 15-day target) straw-plan Deep Argo array (Fig. 1). In section 4 we present the results of these calculations, and we discuss the ramifications in section 5.

2. Data and processing

To evaluate deep and abyssal temperature variance, we use 24 710 CTD stations from 467 full-depth hydrographic sections sampled from 1975 to 2010 (Fig. 2). The data were downloaded from online (http://cchdo.ucsd.edu/) in 2010. The CTD station data used are high vertical (1–2 dbar) resolution and are generally accurate to ±1–2 m°C in temperature, about ±0.002–0.003 PSS-78, and ±3 dbar in pressure, near the Deep Argo accuracy targets. These hydrographic sections are typically occupied at a nominal horizontal resolution of 55 km between stations (55 km is the mode of station spacing in the sections used here), closer over rapidly changing bathymetry (midocean ridges and continental slopes), but occasionally stations are farther apart. The mean station spacing for the sections we use (limiting our

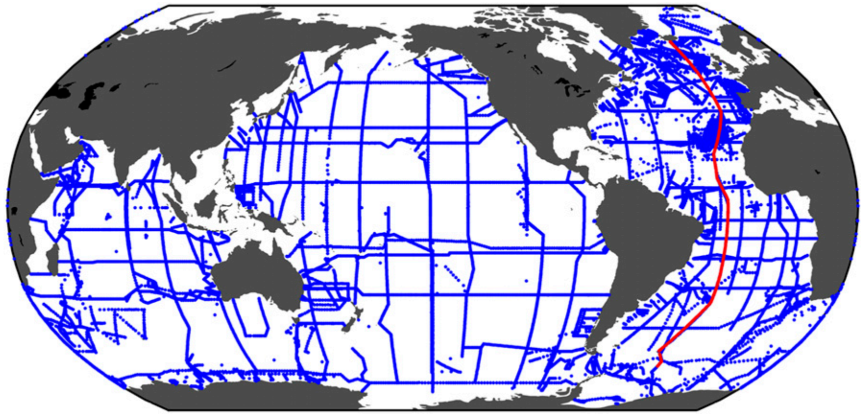

FIG. 2. Map of station positions for the CTD profiles used in this study (blue dots). The WOCE hydrographic section A16 is highlighted by color (red dots).

calculations to regions along the sections where station spacing is <100 km) is 44 km, with a standard deviation of 24 km.

Potential temperature profiles from each station are first low passed vertically using a 20-dbar half-width Hanning filter and subsampled at 50-dbar intervals. Such filtering is often used to remove small vertical-scale features when studying the larger scales, and a vertical resolution of 50 dbar is more than sufficient for quantification of global patterns of deep temperature variance. A minimum of three measurements with a mean distance of 6–2/3 dbar are required within 20 dbar of each interpolated pressure level. The data at each pressure level are then high passed along each hydrographic section using a 500-km loess filter, requiring at least 10 measurements within 500 km of each station location for consideration. The resulting temperature variances at each pressure level are averaged in 5° longitude × 5° latitude bins. Bins with <30 measurements are discarded as potentially unreliable indicators of regional variance.

A comparison of the original 500-km loess low-passed and high-passed temperature data (Fig. 3) along one synoptic hydrographic section illustrates how subtracting the low-passed field (Fig. 3b), an approximation of the smooth long-term mean, from the original field (Fig. 3a) that includes mesoscale eddy signatures leaves only these energetic smaller-scale eddy signatures (Fig. 3c). The particular section shown, a meridional one extending from 60°S to Iceland nominally along 25°W (Fig. 2, red dots), is located in the dynamic western basins of the South Atlantic Ocean and the more quiescent eastern basins of the North Atlantic. This section has been occupied several times. Here we display data (Fig. 3) from the 2005 occupation of the southern portion (Johnson and Doney 2006) and the 2003 occupation of the northern portion (Johnson et al. 2005).

The eddy signatures observed (Fig. 3c) are generally vertically coherent in the deep ocean, resulting in a banded structure that illustrates the ~160-km lateral decorrelation length scale previously estimated from global repeated hydrographic sections (Purkey and Johnson 2010). Eddies are strongest in regions of high vertical gradient (Fig. 3b), such as the deep thermocline between the Antarctic Bottom Water and the North Atlantic Deep Water in the Brazil basin (from 35°S to the equator at around 4000 dbar), as well as in energetic regions, such as the Antarctic Circumpolar Current and western boundary current extension south of 40°S; underneath the North Atlantic Current from 30° to 40°N; and around the equator, where equatorial deep jets (Johnson and Zhang 2003) and the flanking extra-equatorial jets (Gouriou et al. 1999) have strong density signatures. The 500-km smoother does a reasonable job of leaving only large-scale features. Even the apparent undulations in the temperature field shallower than 3000 m from 20°S to 5°S are long-term signatures of zonal currents that are reflected in water property fields such as salinity and dissolved oxygen (Talley and Johnson 1994). However, the large-scale filter likely overestimates eddy variance around narrow boundary currents such as the cold overflow evident on the continental rise from about 59° to 62°N, just south of Iceland (Fig. 3a), and the strong, sharp fronts of the Antarctic Circumpolar Current.

For calculating standard errors, we need estimates of decorrelation time scales in addition to variance. For this purpose, we use Argo float data downloaded from an Argo global data assembly center in January 2015, an initial total of 1 123 092 profiles from 10 090 floats. We consider only profile data with good quality control flags from float cycles with position flags of either good, changed, or interpolated. We linearly interpolate all

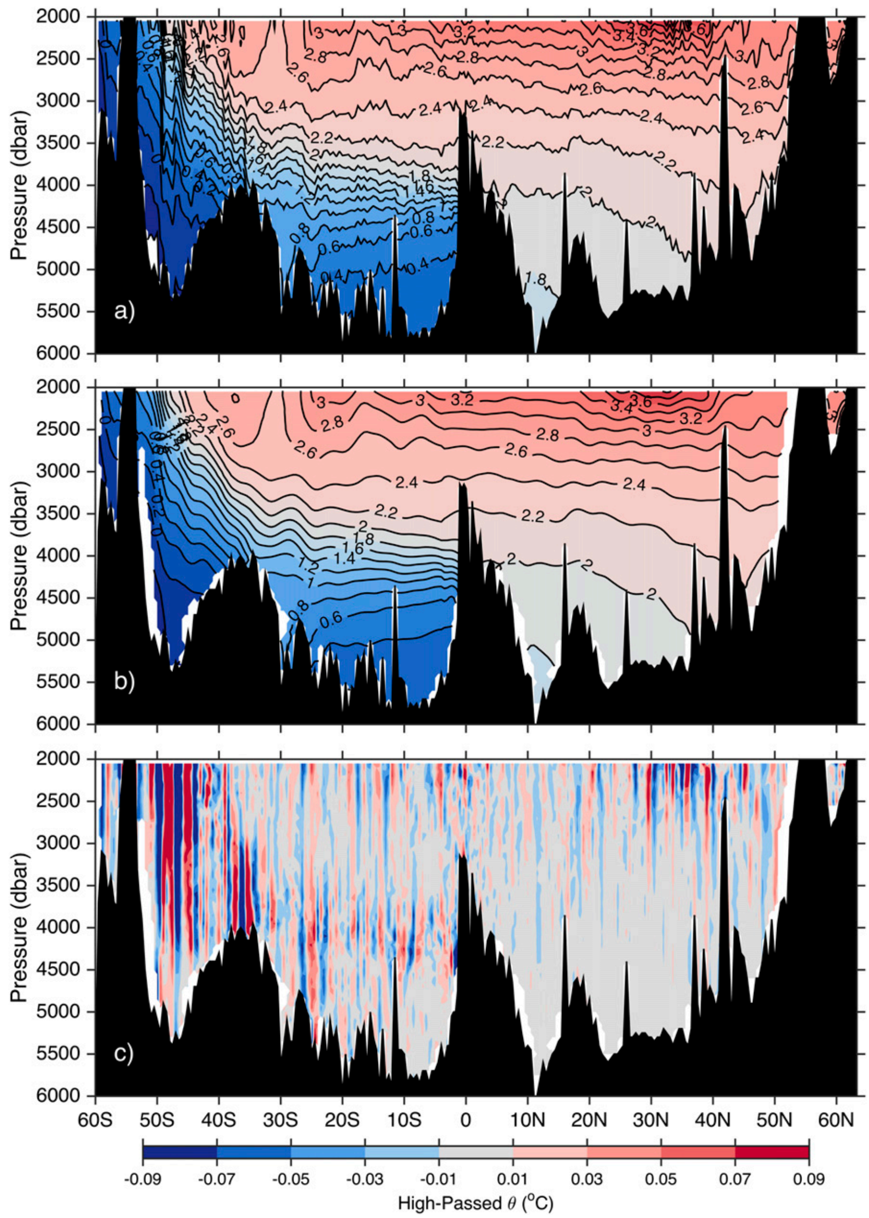

FIG. 3. Pressure–latitude sections of potential temperature along WOCE hydrographic section A16, nominally along 25°W in the Atlantic (Fig. 2, red dots), using the 2003 data in the North Atlantic (Johnson et al. 2005) and the 2005 data in the South Atlantic (Johnson and Doney 2006). (a) The unsmoothed data, contoured at 0.2°C intervals. (b) The data horizontally low-pass filtered using a 500-km loess filter, contoured at the same intervals. (c) The data horizontally high-pass filtered by subtracting (b) from (a), contoured at 0.02°C intervals (see color bar).

data to 1800 dbar, discarding any profiles with vertical measurement spacing more than 200 dbar around that pressure surface.

3. Analysis

We begin by assessing quasi-Langrangian decorrelation time scales for the 1800-dbar temperature anomaly time series for each Argo float. To find the anomalies, we fit a mean, trend, annual cycle, and semiannual cycle to monthly gridded objective maps of Argo temperature data from 2004 to 2014 (Roemmich and Gilson 2009) and subtract these quantities from the float time series at each profile's time and location. These calculations yield a set of time series of temperature anomalies at 1800 dbar for every Argo float.

We consider only time series from floats where the mean time interval between profiles is 12 days or less, the standard deviation of that time interval is one day or less, less than 10% of the profiles for a given float have missing values, and the length of the time series from that float is at least 10 times the estimated decorrelation time scale. This screening retains data from 207 935 profiles from 1575 floats, scattered around the globe. We estimate the decorrelation time scale for each of these 1575 temperature anomaly time series as twice the maximum value of the integral of the normalized autocorrelation sequence for the time series (von Storch and Zwiers 1999). We discuss details of the results in the next section, but the resulting average value of 62 days for all the time series is employed in the calculations described below.

We perform two different types of analyses, local and global, using the estimates of deep temperature variance described above. Both analyses assume a relatively sparse straw-plan Deep Argo array with $5° \times 5° \times$ 15-day sampling. With the present designs of 6000-dbar capable floats, 15-day sampling would provide a balance among the desire for longevity (favoring at least a 5-yr lifetime), concerns about sensor drift (favoring lifetimes not much more than 5 years), and statistical independence of profiles (section 4). Such an array, of about 1228 floats (excluding areas of the ocean shallower than 2000 m or covered by sea ice year-round), would resolve subbasin scales and provide about 30 000 full-depth profiles per year—more data than from the WOCE, CLIVAR, and GO-SHIP hydrographic sections (which took over three decades to collect) analyzed here. The Deep Argo data would also be evenly distributed across the seasons (rather than concentrated in the hemispheric summer as ship-based hydrographic section data are) and more evenly distributed around the globe (rather than sampled densely along quasi-synoptic sections with large gaps between them, as ship-based hydrographic data usually are collected). For the local analyses we estimate statistical uncertainties for local decadal temperature trends. For the global analyses, we estimate statistical uncertainties for global integrals of annual ocean heat content anomalies and annual thermosteric sea level anomalies from 2000 to 6000 dbar.

We assume that at these space scales ($5° \times 5°$), each sample is spatially statistically independent. The 160-km global average lateral decorrelation length scale found using repeat hydrographic section data (Purkey and Johnson 2010) certainly supports this assumption, being considerably shorter than the hypothetically sparsely sampled array for Deep Argo studied here. We also assume that the global mean decorrelation time scale for the deep ocean is about 62 days, the value estimated from the average of Argo float temperature anomaly time series at 1800 dbar.

For both the local and global calculations, we use the variance estimates to calculate yearly uncertainties, assuming that every 2 months of data in each $5° \times 5°$ bin are independent when calculating standard errors of the mean at each location. We then estimate the standard error for a decadal trend (from 10 sequential annual averages) using a weighted least squares linear fit (e.g., Wunsch 1996). The standard error of this fit depends only on the weights used (the inverse of the squared standard errors of the mean), so calculating an actual trend or the residuals is not necessary.

For the local calculations, this exercise is carried out at each pressure level and each grid point, where 30 or more observations from hydrographic sections are available for estimating the temperature variance.

For the global integrals, we linearly interpolate the variance estimates to unsampled or undersampled bins on each horizontal level. However, we do not extrapolate poleward of where we have samples in any ocean. Thus, we scale integrated uncertainties at each pressure level by the ratio of the total ocean volume at each pressure level (determined by the bathymetry) to the sampled ocean volume (determined by bathymetry and the requirement that bins contain 30 or more temperature estimates). For these global integrals, we assume that uncertainties are completely correlated in the vertical. Thus, during the vertical integrals, errors are summed. This assumption is consistent with the vertically banded structure of eddy energy in the synoptic hydrographic sections (Fig. 3c). However, based on the fact that the array density is much less than the average 160-km decorrelation length scale, we also assume that uncertainties are completely uncorrelated laterally; hence, the vertically volume-integrated uncertainties are propagated as the square root of the sum of the squares (i.e., added in quadrature) when integrating horizontally (e.g., Taylor 1980, 68–72). For the global heat content calculations, we assume a constant surface-referenced heat capacity of $3987\ \mathrm{J\,kg^{-1}\,°C^{-1}}$ and a constant in situ density of $1043\ \mathrm{kg\,m^{-3}}$. We estimate these constants from volume-weighted averages for the global ocean deeper than 2000 m using a hydrographic climatology (Gouretski and Koltermann 2004) and the International Equation of State of Seawater (EOS-80). For the uncertainty of the global thermosteric sea level integral, we estimate the local thermal expansion coefficients using the mean observed salinity and temperature values, along with the appropriate pressure value and EOS-80.

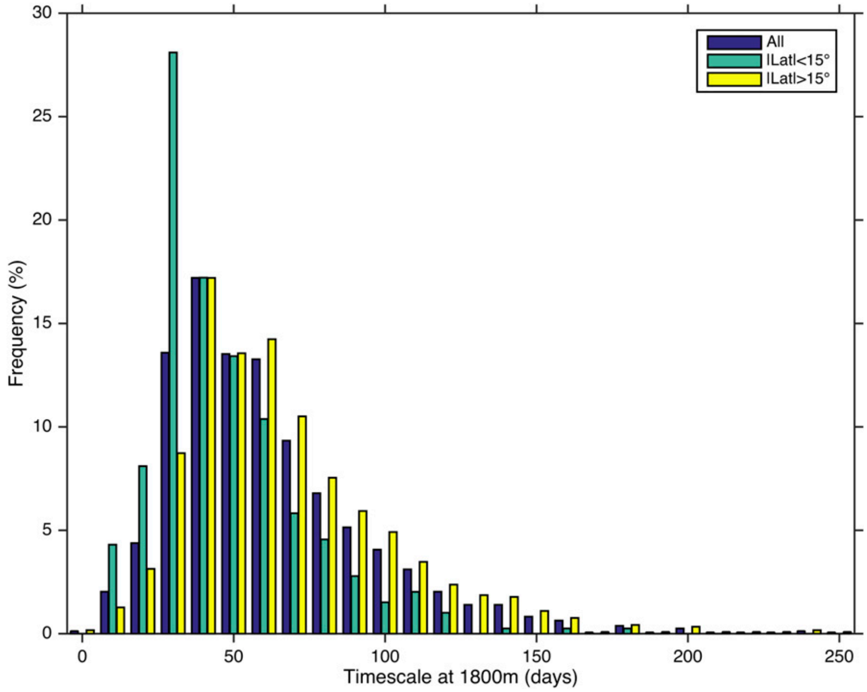

FIG. 4. Histograms of decorrelation time scales in 10-day bins estimated from temperature anomaly time series at 1800 dbar from a screened subset of 1575 Argo floats around the globe (blue bars, left of bin centers; Fig. 5), the 395 floats with mean latitudes within 15° of the equator (green bars, bin centered), and the remaining 1180 with mean latitudes outside of that near-equatorial band (yellow bars, right of bin centers).

4. Results

The quasi-Langrangian decorrelation time scales estimated for the 1800-dbar temperature anomaly time series from Argo floats exhibit a distribution skewed toward longer values (Fig. 4). While the mean time scale is 62 days, the median is only 54 days, and the mode is around 40 days. Only 10% of the values are below 28 days and only 10% exceed 107 days. In addition, there are noticeable spatial variations in the decorrelation time scale (Fig. 5), with lower values in the tropics and along the western boundary of the North Pacific, and higher values in the interior of the North Pacific and at higher latitudes, as might be expected given generally higher eddy energy levels at western boundaries and around the equatorial waveguide. There are slight hints of shorter time scales at the western boundaries of other basins, but the most robust global pattern is shorter time scales within 15° latitude of the equator and slightly longer time scales at higher latitudes (Figs. 4 and 5). The 395 time series with mean latitudes within 15° of the equator have a mean decorrelation time scale of 47 days, a median of 41 days, and a mode around 30 days. The other 1180 time series at higher latitudes have a mean decorrelation time scale of 67 days, a median of 60 days, and a mode around 40 days.

To be conservative, and for simplicity, we assume six independent samples per year for Deep Argo floats, based upon the global mean time scale of 62 days. However, since standard errors scale as the inverse of the square root of the number of independent samples, the results are not overly sensitive to this assumption. Even for a 28-day time scale, estimated uncertainties would only be reduced by about 33%, whereas for a 107-day time scale they would only be inflated by about 31%.

We estimate uncertainties of decadal deep ocean temperature trends for the straw-plan Deep Argo array using the local variances and global mean decorrelation space and time-scale estimates detailed above. The uncertainties vary by an order of magnitude both vertically (Fig. 6) and laterally (Fig. 7). Meridional–vertical sections of zonal averages of uncertainties in decadal temperature trends for the three major oceans (Fig. 6) show a general pattern of decreasing uncertainties with increasing pressure, likely owing to the overall reduction in vertical temperature gradient with increasing depth. There is a maximum in deep uncertainties in the latitude range of the relatively vigorous Antarctic Circumpolar

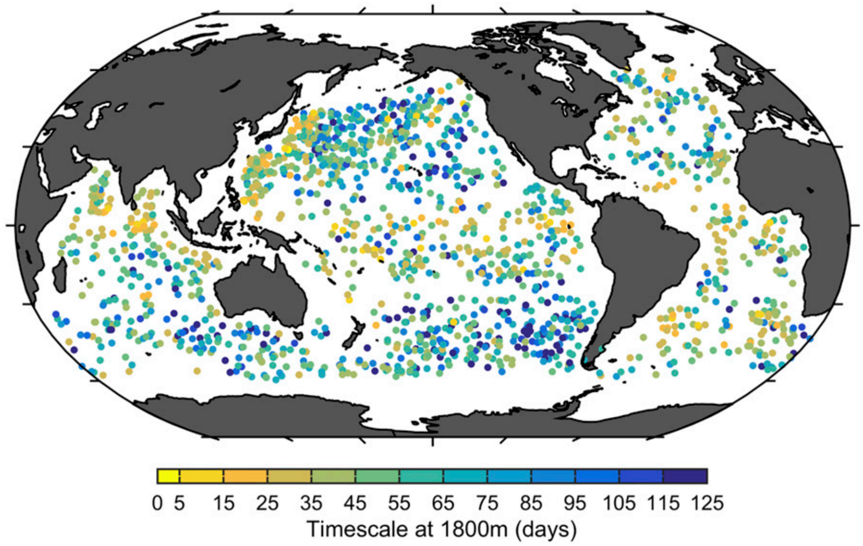

FIG. 5. Decorrelation time scales (color bar) estimated from temperature anomaly time series at 1800 dbar from a screened subset of 1575 Argo floats, plotted at mean locations of the profiles comprising the time series for each Argo float.

Current and western boundary current extensions (60°–40°S), with a meridional maximum of zonally and depth-averaged values below 2000 dbar of 26 m °C decade^{-1} at 50°S. There are also indications of an equatorial maximum in the Atlantic and Pacific Oceans, consistent with the presence of vigorous time-dependent equatorial features, such as the equatorial deep jets (e.g., Youngs and Johnson 2015). The northern North Atlantic, with its deep thermocline and relatively strong deep vertical temperature gradients, also exhibits relatively high values from 30° to 70°N, with lower values in the deep Greenland–Iceland–Norwegian Seas. The abyssal North Pacific Ocean has the lowest uncertainties, in places $<$1 m °C decade^{-1}.

Maps of uncertainties for decadal temperature trends at 3000 and 4000 dbar (Fig. 7) reveal patterns similar to the zonal averages but provide detail as to zonal variations. The eastern portions of the oceans are generally more quiescent than the western portions, as might be expected given the existence of vigorous western boundary currents. The band of high uncertainties associated with the Antarctic Circumpolar Current and the northern North Atlantic, two locations where currents are very deep reaching, are also apparent.

Global integrals of heat content uncertainties for pressures of 2000–6000 dbar have a yearly uncertainty of 1 ZJ (1 ZJ = 10^{21} J) standard error of the mean, resulting in a formal decadal trend standard error of 3 TW (1 TW = 10^{12} W). For the uncertainty of the thermosteric contribution to globally averaged sea level over that same pressure range, the uncertainty is 0.1 mm annually, resulting in a formal decadal trend standard error of $\pm$0.1 mm decade^{-1}.

5. Discussion

Here we estimate quasi-Lagrangian decorrelation time scales from Argo float deep (1800 dbar) temperature anomaly time series. We assess noise levels from temperature variance of 500-km high-passed WOCE and GO-SHIP hydrographic section data averaged in 5° × 5° bins. The spatial pattern of deep decorrelation time scales (Fig. 5) is perhaps not surprising, with shorter values near the eddy-richer western boundaries and around the energetic equatorial waveguide, and longer values in the more quiescent eastern sides of basins at higher latitudes.

The 62-day global mean value of the decorrelation time scales means that for a profiling interval of 15 days, on average about every fourth profile would be independent, resolving some of the temporal variability. Around western boundaries and the equator, each Deep Argo profile might be closer to being a statistically independent sample than on the eastern sides of basins at higher latitudes. One could attempt to use a map of the decorrelation time scales to refine regional uncertainty estimates, but since standard errors scale as the inverse square root of the number of independent samples, the results are not especially sensitive to the use of a mean value instead of a regionally varying one.

While the vertically banded nature of high-passed temperatures in the synoptic hydrographic section data

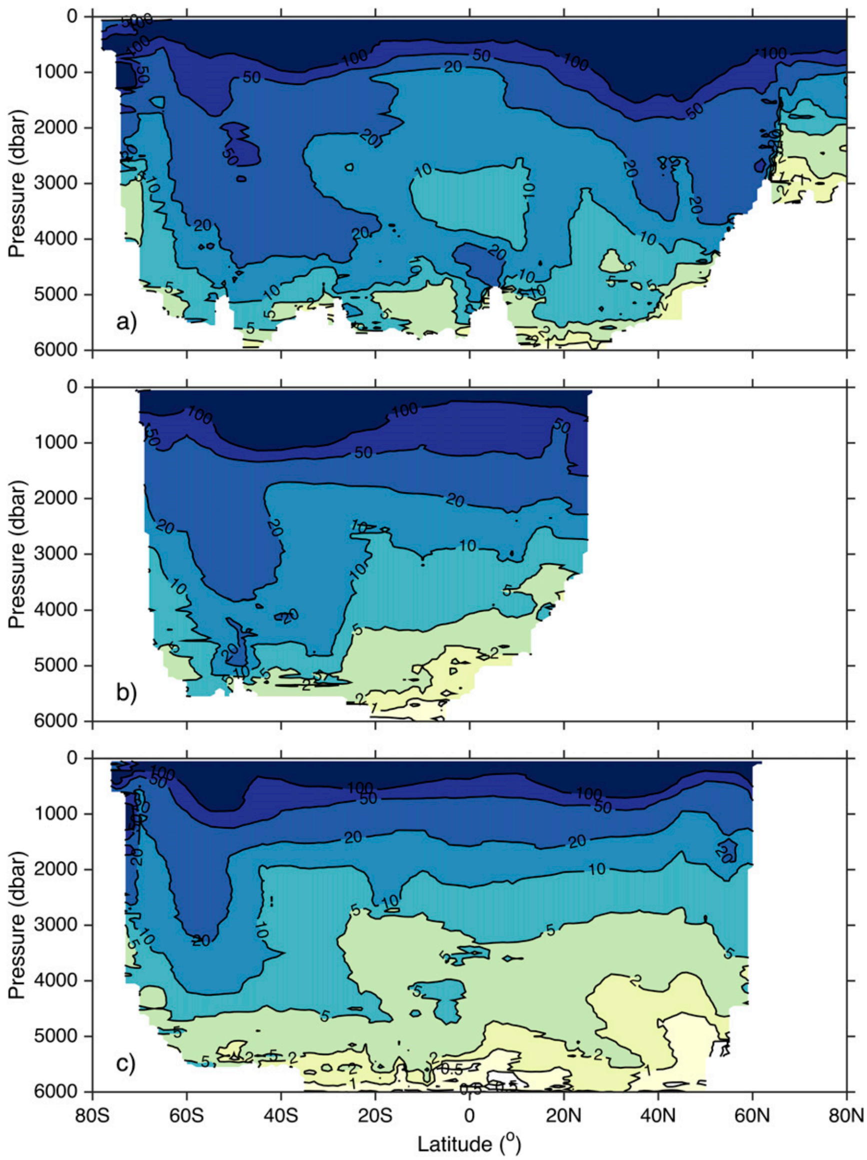

FIG. 6. Meridional–vertical sections (latitude vs pressure) of zonal averages of estimated decadal temperature trend standard errors (m °C decade^{-1}) for the (a) Atlantic, (b) Indian, and (c) Pacific Oceans. Contours (labeled) are at approximately logarithmic intervals.

(e.g., Fig. 3c) suggests the decorrelation time scales at 1800 dbar may be typical of Deep Argo floats at greater depths, it is also possible that different choices of parking depths for the Deep Argo floats, or perhaps the time spent profiling in regions of varying shear, may change the decorrelation time scales from Deep Argo floats compared to those from Argo floats at 1800 m, another argument for simply using the global mean decorrelation time scale.

One could also attempt to estimate decorrelation time scales from deep moored temperature time series, but a few confounding factors would make those less relevant for the study at hand than those estimated from the Argo float time series. First, the decadal time series of Argo data allow removal of estimates of the seasonal cycle from the float time series, something that would not be possible from most moored time series, which are not often longer than a year to two in duration; that inability to remove the seasonal cycle would likely bias the decorrelation time scales from the moored time series toward long values. Second, deep moored temperature records typically do not extend over much more than a year or two, and those short records could hinder robust estimates of decorrelation time scales. Third, vertical

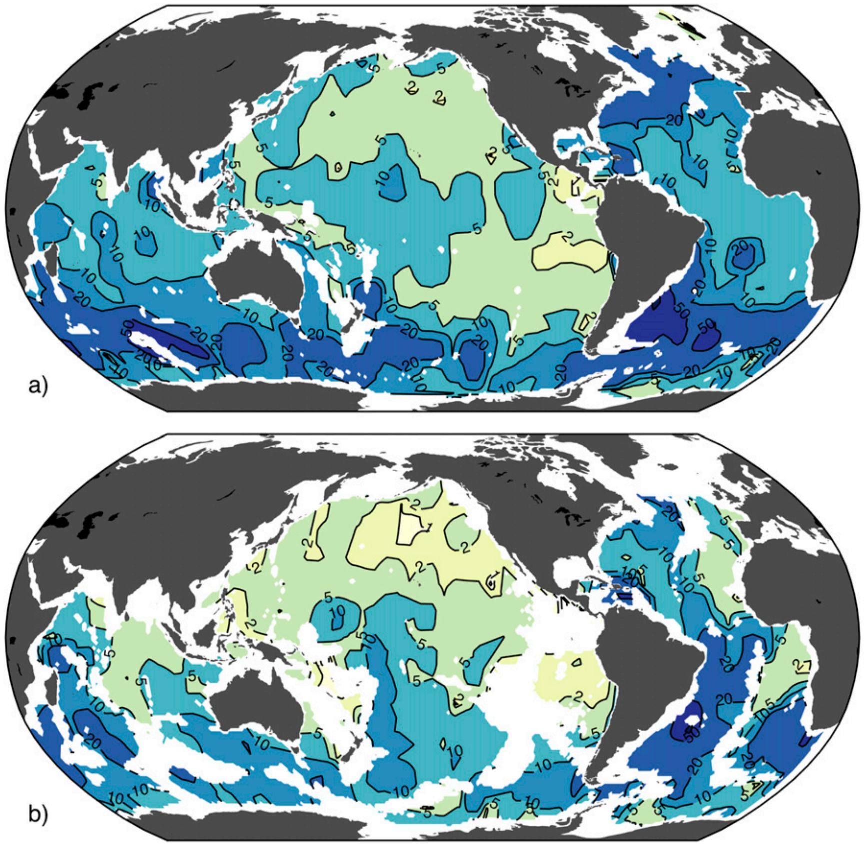

FIG. 7. Maps of estimated temperature trend standard errors (m °C decade^{-1}) at (a) 3000 and (b) 4000 dbar. Bins with fewer than 30 measurements are not included, and values in unsampled or undersampled bins are linearly interpolated from surrounding well-sampled bins. Contours (labeled) are at approximately logarithmic intervals.

mooring motion can introduce spurious variance into temperature records (Meinen 2008), an artifact not present in float profiles. Finally, floats sample temperature close to instantaneously, whereas some current meter data are low passed to filter out higher-frequency variability, so the float data contain variance from these phenomena that would be reduced in low-passed current meter data.

Array design depends on the questions to be answered. Here we cast our findings simply, in terms of local and global decadal trends detectable above one standard error of the mean for a 5° × 5° × 15-day Deep Argo array (Fig. 1) using estimated 160-km spatial and two-monthly temporal decorrelation scales (the latter based on the global mean value of 62 days estimated using temperature anomaly time series at 1800 dbar from Argo floats). Such an array would be capable of resolving, on average, local trends of <1 m °C decade^{-1} in the abyssal Pacific and at worst around 26 m °C decade^{-1} zonally and depth averaged below 2000 dbar along 50°S, in the energetic deep Southern Ocean. Decadal trends from 1992 to 2005 have been estimated at 5 m °C decade^{-1} in the global abyssal ocean, and 30 m °C decade^{-1} in the deep Southern Ocean using repeat hydrographic data (Purkey and Johnson 2010); that analysis required large-scale (basin, ocean, or global) averages to find statistically significant results. In contrast, the straw-plan Deep Argo array would be capable of detecting anticipated decadal trends *locally* at 5° × 5° resolution on decadal time scales.

The trend in deep (>2000 dbar) global ocean heat gain from 1992 to 2005 was assessed at +35 (±17) TW (one standard error uncertainty) using repeat hydrographic data (Purkey and Johnson 2010). The deep (>2000 dbar) global ocean trend in heat gain for 2005–13 is estimated at −40 (±220) TW (one standard error uncertainty) from a residual of 0–2000-m Argo steric expansion, ocean mass change estimates from GRACE satellite gravimetry, and ocean sea level change estimates from satellite altimetry (Llovel et al. 2014). The straw-plan Argo array here, fully implemented for a decade, could provide annual values to within a yearly one standard error uncertainty of 1 ZJ and hence a deep (>2000 dbar) global ocean heat decadal trend to within ±3 TW—a large improvement over the direct estimate from repeat hydrography and a huge improvement over the residual calculation.

Similarly, the contribution of deep (>2000 dbar) ocean thermal expansion to global sea level rise could be determined to a standard error of 0.1 mm annually, with a trend standard error of ±0.1 mm decade^{-1}. These numbers compare with a repeat hydrographic trend standard error of ±0.5 mm decade^{-1} (Purkey and Johnson 2010) and a trend standard error of ±7 mm decade^{-1} for the satellite–Argo residual calculation (Llovel et al. 2014). These full-depth steric expansion fields, together with sea surface height fields from satellite altimetry, would allow a very precise assessment of spatiotemporal variations in sea level, including those expected from changes in the gravity field with melting glaciers and ice sheets (Bamber and Riva 2010).

There are certainly other benefits of a Deep Argo array that are not assessed here. As mentioned in the introduction, there are considerable changes observed in the deep meridional overturning circulation of both the North Atlantic Deep Water and the Antarctic Bottom Water in recent decades, but these are sampled only decadally by repeat hydrographic sections (Purkey and Johnson 2012) or locally by moored arrays (Smeed et al. 2014). Deep Argo would measure these changes globally and continuously. In addition, there are large salinity changes in the components of North Atlantic Deep Water (Yashayaev 2007), as well as Antarctic Bottom Water in the Pacific (Swift and Orsi 2012), Indian (Aoki et al. 2005), and perhaps even Atlantic (Jullion et al. 2013) Oceans that Deep Argo would also measure globally and continuously.

Deep Argo data would complement, and not supplant, repeat hydrographic section data. Repeat hydrographic section data provide the highly accurate and traceable salinity data required to check and adjust Argo (and Deep Argo) conductivity sensor data (Wong et al. 2003). Furthermore, repeat hydrographic sections, when quasi synoptic, full depth, and coast to coast, allow for well-constrained transport estimates, including boundary currents (Ganachaud 2003), that Argo and Deep Argo resolve less well. Repeat hydrographic sections also collect data on other water properties that allow for direct estimates of ocean carbon uptake (Sabine and Tanhua 2010), ocean acidification, (Byrne et al. 2010), and long-term changes in dissolved oxygen concentration (Stramma et al. 2008), as well as estimates of changes in ocean circulation and ventilation from transient tracers (Fine 2011). Deep Argo would provide well-resolved temperature, salinity, and perhaps dissolved oxygen fields, allowing improved inventory estimates for ocean water properties when combined with the repeat hydrographic section data.

Acknowledgments. We thank everyone who helped to collect, calibrate, process, and archive the WOCE, CLIVAR, and GO-SHIP hydrographic section data. Argo data are collected and made freely available by the international Argo program, which is part of the Global Ocean Observing System, and the national programs that contribute to it (http://www.argo.ucsd.edu, http://argo.jcommops.org). GCJ and JML are supported by the NOAA Climate Program Office and NOAA research. SGP is supported through an LDEO postdoctoral fellowship.

REFERENCES

Aoki, S., S. R. Rintoul, S. Ushio, S. Watanabe, and N. L. Bindoff, 2005: Freshening of the Adélie Land Bottom Water near 140°E. *Geophys. Res. Lett.*, **32**, L23601, doi:10.1029/2005GL024246.

Bamber, J., and R. Riva, 2010: The sea level fingerprint of recent ice mass fluxes. *Cryosphere*, **4**, 621–627, doi:10.5194/tc-4-621-2010.

Byrne, R. H., S. Mecking, R. A. Feely, and X. Liu, 2010: Direct observations of basin-wide acidification of the North Pacific Ocean. *Geophys. Res. Lett.*, **37**, L02601, doi:10.1029/2009GL040999.

Cunningham, S. A., and Coauthors, 2013: Atlantic Meridional Overturning Circulation slowdown cooled the subtropical ocean. *Geophys. Res. Lett.*, **40**, 6202–6207, doi:10.1002/2013GL058464.

Dieng, H. B., H. Palanisamy, A. Cazenave, B. Meyssignac, and K. von Schuckmann, 2015: The sea level budget since 2003: Inference on the deep ocean heat content. *Surv. Geophys.*, **36**, 209–229, doi:10.1007/s10712-015-9314-6.

Fine, R. A., 2011: Observations of CFCs and SF_6 as ocean tracers. *Annu. Rev. Mar. Sci.*, **3**, 173–195, doi:10.1146/annurev.marine.010908.163933.

Ganachaud, A., 2003: Large-scale mass transports, water mass formation, and diffusivities estimated from World Ocean Circulation Experiment (WOCE) hydrographic data. *J. Geophys. Res.*, **108**, 3213, doi:10.1029/2002JC001565.

Gordon, A. L., 1982: Weddell Deep Water variability. *J. Mar. Res.*, **40**, 199–217.

Gouretski, V. V., and K. P. Koltermann, 2004: WOCE global hydrographic climatology. Berichte des Bundesamtes fur Seeschifffahrt und Hydrographie 35/2004, 52 pp.

Gouriou, Y., B. Bourlès, H. Mercier, and R. Chuchla, 1999: Deep jets in the equatorial Atlantic Ocean. *J. Geophys. Res.*, **104**, 21 217–21 226, doi:10.1029/1999JC900057.

Johnson, G. C., 2008: Quantifying Antarctic Bottom Water and North Atlantic Deep Water volumes. *J. Geophys. Res.*, **113**, C05027, doi:10.1029/2007JC004477.

——, and D. Zhang, 2003: Structure of the Atlantic Ocean equatorial deep jets. *J. Phys. Oceanogr.*, **33**, 600–609, doi:10.1175/1520-0485(2003)033<0600:SOTAOE>2.0.CO;2.

——, and S. C. Doney, 2006: Recent western South Atlantic bottom water warming. *Geophys. Res. Lett.*, **33**, L14614, doi:10.1029/

2006GL026769; Corrigendum, **33**, L21604, doi:10.1029/2006GL028294.

——, and J. M. Lyman, 2014: Oceanography: Where's the heat? *Nat. Climate Change*, **4**, 956–957, doi:10.1038/nclimate2409.

——, J. L. Bullister, and N. Gruber, 2005: Labrador Sea Water property variations in the northeastern Atlantic Ocean. *Geophys. Res. Lett.*, **32**, L07602, doi:10.1029/2005GL022404.

Jullion, L., A. C. Naveira Garabato, M. P. Meredith, P. R. Holland, P. Courtois, and B. A. King, 2013: Decadal freshening of the Antarctic Bottom Water exported from the Weddell Sea. *J. Climate*, **26**, 8111–8125, doi:10.1175/JCLI-D-12-00765.1.

Klatt, O., O. Boebel, and E. Fahrbach, 2007: A profiling float's sense of ice. *J. Atmos. Oceanic Technol.*, **24**, 1301–1308, doi:10.1175/JTECH2026.1.

Kouketsu, S., and Coauthors, 2011: Deep ocean heat content changes estimated from observation and reanalysis product and their influence on sea level change. *J. Geophys. Res.*, **116**, C03012, doi:10.1029/2010JC006464.

Llovel, W., J. K. Willis, F. W. Landerer, and I. Fukumori, 2014: Deep-ocean contribution to sea level and energy budget not detectable over the past decade. *Nat. Climate Change*, **4**, 1031–1035, doi:10.1038/nclimate2387.

Lumpkin, R., and K. Speer, 2007: Global ocean meridional overturning. *J. Phys. Oceanogr.*, **37**, 2550–2562, doi:10.1175/JPO3130.1.

Mauritzen, C., A. Melsom, and R. T. Sutton, 2012: Importance of density-compensated temperature change for deep North Atlantic Ocean heat uptake. *Nat. Geosci.*, **5**, 905–910, doi:10.1038/ngeo1639.

Meinen, C. S., 2008: Accuracy in mooring motion temperature corrections. *J. Atmos. Oceanic Technol.*, **25**, 2293–2303, doi:10.1175/2008JTECHO555.1.

Msadek, R., C. Frankignoul, and L. Z. X. Li, 2011: Mechanisms of the atmospheric response to North Atlantic multidecadal variability: A model study. *Climate Dyn.*, **36**, 1255–1276, doi:10.1007/s00382-010-0958-0.

Orsi, A. H., G. C. Johnson, and J. L. Bullister, 1999: Circulation, mixing, and production of Antarctic Bottom Water. *Prog. Oceanogr.*, **43**, 55–109, doi:10.1016/S0079-6611(99)00004-X.

Purkey, S. G., and G. C. Johnson, 2010: Warming of global abyssal and deep Southern Ocean waters between the 1990s and 2000s: Contributions to global heat and sea level rise budgets. *J. Climate*, **23**, 6336–6351, doi:10.1175/2010JCLI3682.1.

——, and ——, 2012: Global contraction of Antarctic Bottom Water between the 1980s and 2000s. *J. Climate*, **25**, 5830–5844, doi:10.1175/JCLI-D-11-00612.1.

Rhein, M., and Coauthors, 2013: Observations: Ocean. *Climate Change 2013: The Physical Science Basis*, T. F. Stocker et al., Eds., Cambridge University Press, 255–315.

Robson, J. I., R. T. Sutton, and D. M. Smith, 2012: Initialized decadal predictions of the rapid warming of the North Atlantic Ocean in the mid 1990s. *Geophys. Res. Lett.*, **39**, L19713, doi:10.1029/2012GL053370.

Roemmich, D., and J. Gilson, 2009: The 2004–2008 mean and annual cycle of temperature, salinity, and steric height in the global ocean from the Argo Program. *Prog. Oceanogr.*, **82**, 81–100, doi:10.1016/j.pocean.2009.03.004.

——, and Coauthors, 2009: The Argo Program: Observing the global ocean with profiling floats. *Oceanography*, **22**, 34–43, doi:10.5670/oceanog.2009.36.

——, J. Church, J. Gilson, D. Monselesan, P. Sutton, and S. Wijffels, 2015: Unabated planetary warming and its ocean structure since 2006. *Nat. Climate Change*, **5**, 240–245, doi:10.1038/nclimate2513.

Sabine, C. L., and T. Tanhua, 2010: Estimation of anthropogenic CO_2 inventories in the ocean. *Annu. Rev. Mar. Sci.*, **2**, 175–198, doi:10.1146/annurev-marine-120308-080947.

Smeed, D. A., and Coauthors, 2014: Observed decline of the Atlantic meridional overturning circulation 2004–2012. *Ocean Sci.*, **10**, 29–38, doi:10.5194/os-10-29-2014.

Smith, T. M., R. W. Reynolds, T. C. Peterson, and J. Lawrimore, 2008: Improvements to NOAA's historical merged land–ocean surface temperature analysis (1880–2006). *J. Climate*, **21**, 2283–2296, doi:10.1175/2007JCLI2100.1.

Somavilla, R., U. Schauer, and G. Budéus, 2013: Increasing amount of Arctic Ocean deep waters in the Greenland Sea. *Geophys. Res. Lett.*, **40**, 4361–4366, doi:10.1002/grl.50775.

Stramma, L., G. C. Johnson, J. Sprintall, and V. Mohrholz, 2008: Expanding oxygen-minimum zones in the tropical oceans. *Science*, **320**, 655–658, doi:10.1126/science.1153847.

Swift, J. H., and A. H. Orsi, 2012: Sixty-four days of hydrography and storms: RVIB *Nathaniel B. Palmer's* 2011 S04P Cruise. *Oceanography*, **25**, 54–55, doi:10.5670/oceanog.2012.74.

Talley, L. D., and G. C. Johnson, 1994: Deep, zonal subequatorial currents. *Science*, **263**, 1125–1128, doi:10.1126/science.263.5150.1125.

——, and Coauthors, 2015: Changes in ocean heat, carbon content, and ventilation: Review of the first decade of GO-SHIP global repeat hydrography. *Annu. Rev. Mar. Sci.*, doi:10.1146/annurev-marine-052915-10082, in press.

Taylor, J. R., 1980: *An Introduction to Error Analysis: The Study of Uncertainties in Physical Measurements*. University Science Books, 272 pp.

Toole, J. M., R. A. Krishfield, M.-L. Timmermans, and A. Proshutinsky, 2011: The ice-tethered profiler: Argo of the Arctic. *Oceanography*, **24**, 126–135, doi:10.5670/oceanog.2011.64.

von Storch, H., and F. W. Zwiers, 1999: *Statistical Analysis in Climate Research*. Cambridge University Press, 484 pp.

Wong, A. P. S., G. C. Johnson, and W. B. Owens, 2003: Delayed-mode calibration of autonomous CTD profiling float salinity data by θ–S climatology. *J. Atmos. Oceanic Technol.*, **20**, 308–318, doi:10.1175/1520-0426(2003)020<0308:DMCOAC>2.0.CO;2.

Wunsch, C., 1996: *The Ocean Circulation Inverse Problem*. Cambridge University Press, 442 pp.

Yashayaev, I., 2007: Hydrographic changes in the Labrador Sea, 1960-2005. *Prog. Oceanogr.*, **73**, 242–276, doi:10.1016/j.pocean.2007.04.015.

Yeager, S., A. Karspeck, G. Danabasoglu, J. Tribbia, and H. Y. Teng, 2012: A decadal prediction case study: Late twentieth-century North Atlantic Ocean heat content. *J. Climate*, **25**, 5173–5189, doi:10.1175/JCLI-D-11-00595.1.

Youngs, M. K., and G. C. Johnson, 2015: Basin-wavelength equatorial deep jet signals across three oceans. *J. Phys. Oceanogr.*, **45**, 2134–2148, doi:10.1175/JPO-D-14-0181.1.